DOI 10.4149/BLL_2024_24

Bratisl Med J 2024; 125 (3):
196–205

EXPERIMENTAL STUDY

An optimized framework for prediagnosis of diabetic retinopathy using HHO-CBL model

Sathyavani ADDANKI, Sumathi D

School of Computer Science and Engineering, VIT-AP University, Amaravati, Andhra Pradesh, India.
sumathi.research28@gmail.com

ABSTRACT
BACKGROUND: Diabetic Retinopathy (DR) is a widespread intense stage of diabetes mellitus that causes vision-effecting anomalies in the retina. It is a medical health condition on the strength of fluctuating glucose level in the blood that can result in vision loss in case of severity.
OBJECTIVE: As a result, early detection and treatment with DR is the most significant task which will tremendously reduce the likelihood of vision impairment and is still a difficult challenge. Many conventional methods fail to detect primary causes of formation of Microaneurysms, that are used to determine the Prediagnosis of DR.
METHOD: To overcome this challenge, the proposed model incorporates Harris Hawk Optimization with CNN-Bi-LSTM (HHO-CBL) to extract the features. The Prediagnosis of DR has been achieved through this model by spotting saccular dilations, hyaline like material in the capillary aneurysm wall, kinking of vessels since these are the indications for the creation of microaneurysms that are spotted in the blood vessel of the retina. The recommended model is also used to automatically detect DR and its progression in many phases. Furthermore, in order to identify the severity of DR retina, we used a benchmark Kaggle APTOS dataset to train the HHO-CBL model.
RESULTS: Experimental results reveal that this model obtains the best classification accuracy of 96.4 % for an early diagnosis and 98.8 % for a five-degree classification. In addition to those results, a comparison with previously carried out studies has also shown that this model provides a promising solution for a successful Prediagnosis of DR and its staging.
CONCLUSIONS: In the current research, an innovative HHO-CBL was developed for identifying the primary causes that lead to the formation of microaneurysms and diagnosing all five grades of DR. According to the acquired results presented through the evaluation performance metrics indicates that the pre-early diagnosis and five grade classification using feature embedding technique outperformed the other prevailing approaches *(Tab. 4, Fig. 10, Ref. 31). Text in PDF www.elis.sk*
KEY WORDS: diabetic retinopathy, Harris Hawk optimization, kinking, hyaline structures, saccular dilations.

Introduction

DR is a condition of the eye that impacts the retina in individuals with diabetes, resulting from damage to the tiny blood vessels due to high blood sugar levels shown in Figure 1 and is typically asymptomatic until it is advanced (1–4).

DR develops in four main stages, ophthalmologists classify diabetic retinopathy (DR) into two stages (5): background retinopathy, also referred to as Non-Proliferative Diabetic Retinopathy (NPDR), and Proliferative Diabetic Retinopathy (PDR). Additionally, NPDR is classified into three stages: A) Mild, B) Moderate, C) Severe as shown in Table 1.

School of Computer Science and Engineering, VIT-AP University, Amaravati, Andhra Pradesh, India

Address for correspondence: Sumathi D, Prof, School of Computer Science and Engineering, VIT-AP University, Amaravati, Andhra Pradesh, India.
Phone: +918778542153

Since DR is so prevalent it is necessary to design and develop reliable tools for its diagnosis. The use of Artificial Intelligence (AI) has had a significant impact on the medical industry during the last several decades, which has led to the development of a wide variety of AI-based methods for medical image interpretation (7). Many approaches for detecting diabetic retinopathy using computer vision have previously been developed.

Most of these techniques fail to reliably recognize mild stage (8–20). Early diagnosis of the condition is essential to forestall blindness and hence it is of utmost importance to detect the mild stage and its primary causes. In the mild stage of NPDR, microaneurysms occur due to local structural weakening in the vessel wall (21). In most cases, microaneurysms were located in the posterior part of the retina, approximately adjacent to the capillaries. In this view weakness of the vessel wall triggers dilations and proliferations that fallows as secondary effect. This study is concerned with the factors, structure, and development of the diabetic retinal microaneurysms. As part of our research in looking for causes of microaneurysms, includes saccular dilations

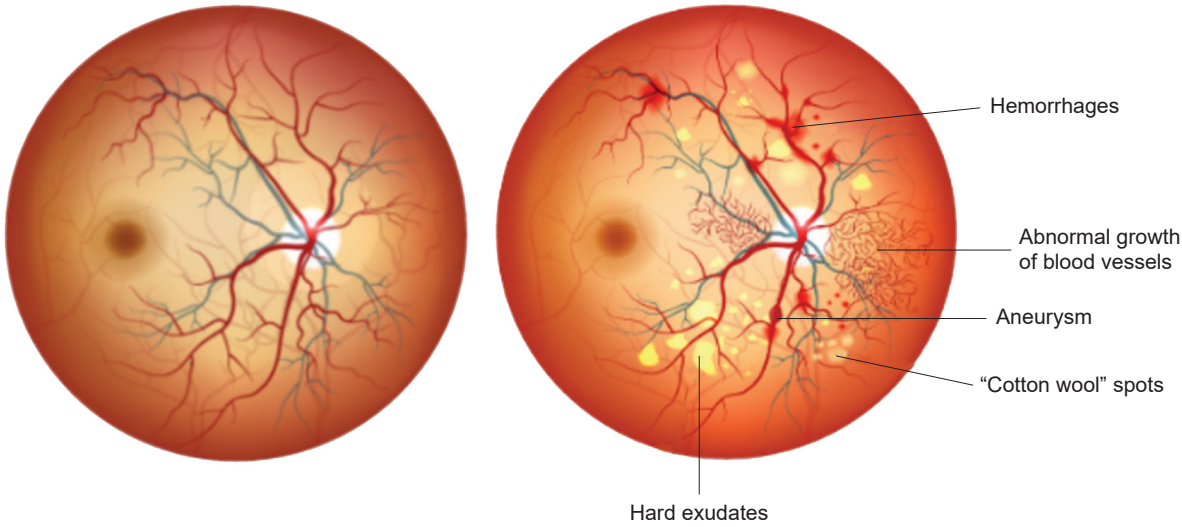

Fig. 1. Healthy and DR affected Retina with lesions (6).

or capillary microaneurysms originating from retinal capillaries. The rise in venous pressure, which is induced by occlusion of thinner retinal veins, and the additional local deterioration of the capillary wall, which is triggered by endothelial deterioration, are the root causes of saccular dilation. Another factor that contributes to the development of microaneurysms is the progressive accumulation of a hyaline like material in the capillary aneurysm wall. Microaneurysms form initially due to a splitting of the capillary basement membrane. The bridge-like linkages are responsible for the characteristic kinking that is seen in the early stages of the creation of microaneurysms. This kinking is caused by direct pull as a consequence of retinal swelling, which is well-known to occur early on in Diabetic Retinopathy (22). So, an end-to-end deep ensemble model is proposed that detects the fundamental causes of initial stages and also classifies all the five phases of the disease.

In this research, we design a framework based on CNN models to solve the challenges stated below. The primary contributions of the proposed approach are

1) A novel architecture utilizing the CNN-Bi-LSTM algorithm is introduced to effectively detect pre-early-stage lesions of diabetic retinopathy (DR) and accurately identify the severity level based on a five-class classification system. For reliable DR grading and early diagnosis, the proposed HHO-CBL model incorporates a Harris Hawk optimization strategy to learn deep visual properties of retinal samples.
2) The proposed method is able to identify the key contributors to the formation of diabetic retinal microaneurysms.
3) The suggested framework identifies the earliest stage of Diabetic Retinopathy, before microaneurysms are formed, by identifying signs of saccular dilation, splitting of the capillary basement membrane, accumulation of a hyaline-like substance, and the typical kinking of blood vessels.
4) The HHO-CBL approach collaboratively utilizes the parameters of a CNN model to classify images for diabetic retinopathy (DR) analysis and evaluation. It offers the advantage of identifying samples through a backward-forward pass, resulting in modifications to the model parameters to facilitate the learning of lesions and images.
5) In this study, a distinct neural network architecture was proposed, which exhibits computational efficiency, achieves superior classification results, and requires relatively less memory and computing time.

The remaining part of this paper is categorized as: Section 2 describes the related work; Sections 3&4 describe the Research gap & Motivation; Section 5 describes the materials and dataset the proposed methodology of diagnostic model; Section 6 describes the Experimental results and the outcomes of the model; Section 7 describes the conclusion of the models.

Methodology

Channeling

Fundus image is typically referred as an RGB images. The red, green, and blue components will be taken from every image. When the structure of the retinal picture is analyzed in each channel, if the lesion is not found in the first channel, the process will go to the next channel to look for it. If the lesion is not found in the second channel, the process will proceed to the final channel once again.

Tab. 1. Clinical Classification of DR.

Levels of DR	Examination of fundus images
No DR	No abnormalities
Non-proliferative DR, Mild	Microaneurysms are identified
Moderate	Along with microaneurysms some hard exudates or bleeding spots are observed
Severe	Blood vessels are blocked, new blood vessels are generated, retinal hemorrhages
Proliferative diabetic retinopathy	Vitreous hemorrhage, retinal detachment, Vision Loss

Hessian matrix

This technique was utilized to identify the image's vascular (tubular) components. The vascularity of the related region is evaluated by taking into consideration all the eigenvalues of the Hessian matrix (23). These values may be computed by performing second-order partial derivatives in a horizontal, vertical, and diagonal direction, respectively. Therefore, tiny tubular geometric structures are identified in an image. A measurement scale that can be adjusted within a predetermined range is defined in the equation (1) due to the fact that vessel sizes might vary considerably.

$$F(x) = max_{\sigma} f(x, \sigma) \tag{1}$$

Thus, x is the position of the image pixel, f is the filter that was applied to the picture to extract the blood vessels, and σ is the standard deviation of the Gauss function that was used to calculate the second order derivative of the image. The goal of this analysis is to determine the horizontal gradient and the vertical gradient that are again differentiated to obtain the second order derivative. Equation (2) gives the structure of the eigenvalues of the Hessian matrix.

$$H = \begin{pmatrix} I_{xx} & I_{xy} \\ I_{yx} & I_{yy} \end{pmatrix} \tag{2}$$

The Hessian Matrix is created by computing the four components of the second order derivative. Consider Ix and Iy be the gradient of the source image in the horizontal and vertical direction correspondingly, and Ixx, Iyy, Ixy, Iyx, represents the second order derivatives. The vascularity index of a vessel may be measured by computing the neighbors of an x pixel that belongs to the vessel and using the eigenvalue of the H matrix.

In Hessian Matrix H, all the principal diagonal is set to some threshold value to compare the pixel values, based on their variance with respect to the principle diagonal elements threshold the severity of disease is diagnosed. If no major change is found in one channel, move to another two channels of an image. If major change is identified in any of the channels that image is given to the Harris Hawk Optimization technique for best feature selection.

Harris Hawks optimization (HHO)

After a vector matrix is generated by Hessian matrix, a sophisticated meta-heuristic optimization technique known as the Harris Hawks Optimization (HHO) technique is applied in order to optimally select the features as a means to enhance classification performance and efficiency. In general, the HHO is one of the population-based gradients-free optimization mechanisms that is widely used in a variety of applications for the purpose of resolving challenging optimization issues (24). In addition, this method incorporates both the phase of exploration and the phase of exploitation, with the exploration phase being completed well before exploitation phase. At this phase, the Harris Hawks are able to recognize and locate their prey by using the strong vision they possess. It outperforms other optimization strategies in terms of convergence rate, efficiency, and a shorter number of iterations required to arrive at the best possible optimum solution. The Hawks and the Harris are regarded to be the best solutions under this process, in which each stage is related to the right prey for the candidate solution (25). Following the initialization of the parameters, the position vector of the hawks is calculated with the help of the following model as shown in the equation (3):

$$Q(s+1) = \begin{cases} Q_{Rh}(s) - r1|Q_{Rb}(s) - 2r_2 C(s)| x < 0.5 \\ (Q_{Rb}(s) - Q_{Avp}(s)) - r3(L_B + r4(U_B - L_B)) x < 0.5 \end{cases} \tag{3}$$

Where, Q(s+1) indicates the following iterations of hawk's position, Q_{Rb} (s)indicates position of rabbit, r1, r2, r3, r4, x are the random numbers of (0,1), Q_{Avp} refers the average position, Q_{Rh} hawk was chosen at random from the present population. Upper and Lower Bounds are denoted by UB and LB.

Next, the simulated rabbit movements are influenced by the random values at each iteration. When the arbitrary location has been established, the average distance value is calculated, taking into account a range of factors. In addition, the intended length of momentum was computed by using the lower bound in the rule. The components of the random scaling coefficient are also considered while designing new patterns for the designated areas. As a result, the hawks settle into the final average position shown in below equation (4):

$$Q_{Avp}(s) = \frac{1}{No_{Hw}} \sum_{i=1}^{No_{Hw}} Q_i(s) \tag{4}$$

Where No_{Hw} is the total number of hawks and Q_i (s) is the coordinates of where each hawk is at time steps. The median position has been calculated using the fewest number of arbitrary rules. This model also incorporates for exploration and exploitation potentials since energy is lost in the following ways given in the equation (5):

$$P_E = 2P_{E0}(1 - \frac{m}{M}) \tag{5}$$

The escape energy of the prey is denoted by P_E the starting energy level is denoted by P_{E0} , and the maximum number of repetitions is denoted by M. The following guidelines are used in this model to predict the hawks' actions illustrated in equation (6, 7):

$$Q(s+1) = \Delta Q(s) - P_E|GQ_{Rb}(s) - Q(s) \tag{6}$$

$$\Delta Q(s) = Q_{Rb}(s) - Q(s) \tag{7}$$

In this case, the current position of the rabbit at iteration k is denoted by ΔQ(s). Then, the following model is applied to update present location represented in the equation (8):

$$Q(s+1) = Q_{Rb}(s) - R_E|\Delta Q(s) \tag{8}$$

The best possible fitness value is calculated using the updated position. Moreover, by selecting the characteristics optimally, the

dimensionality of features has been minimized, and the significance of each feature to the whole has been verified in the following ways equation (9):

$$MutualS(G, CF) = \frac{1}{|G|}\sum_{Re_F \in CF} H(Re_F, CF) \quad (9)$$

Where Mutuals(G, CF)signifies the mutual significance, CF is the common feature, Re_F specifies the relevant feature, and G is regarded to be the chosen function with fitness value. This operation is used to determine the most optimal function to choose the most appropriate features, which can then be utilized for training the classifier (26).

HHO-CBL model

CNNs have emerged as the preferred deep learning algorithms for training medical images and classifying abnormalities within them. This preference stems from their ability to preserve crucial features and spatial relationships during image analysis. In the context of retinal images, for instance, identifying key details like the onset of blood vessel ruptures or the accumulation of yellow fluid near the macular region is of utmost significance (27).

In this network, optimized features selected from the HHO optimization technique are given to integrated deep architecture (Convolutional Neural Network and Bidirectional Long Short-Term Memory) as shown in the (28). The developed network has seven convolutional layers, four max pooling layers, four Rectified Linear Unit (ReLU) and three Exponential Linear Unit (ELU) activation functions, one flattens layer, two Fully Connected Layers (FCLs), and one SoftMax layer. Additionally, there are two Bi-LSTM layers. Convolutional and pooling structures have been employed in the suggested architecture to extract complicated features from pictures. This was implemented to enhance the extraction accuracy. In order to investigate the temporal properties of the extracted features, the Bi-LSTM layer provides a brief overview of the proposed CNN-Bi-LSTM neural network. The proposed network has a 256 x 256 x 3pixel input size. Therefore, the input picture has been scaled to 256x563 before being fed into the proposed network. Specifically, the conv layers in the given network have been activated using the ReLU and ELU functions (29). In addition, it should be mentioned that the kernel size in the conv layer has been maintained at 3*3, while that in the max-pool layer has been kept as 2*2. Following that, output of Fully Connected Layer (FC1) has been fed into two further Bi-LSTM layers, which are referred to as BiLSTM6 and BiLSTM7, respectively. It is significant noted that the output of FC5 has been flattened by a flatten layer before it has been provided as input to the Bi-LSTM layers. As a result of this, the output of FC5 has been prepared to serve as the input for the BiLSTM6 layer. It is required to mention that the state activation function and the gate activation function in the Bi-LSTM layers have both been retained as tanh and sigmoid, respectively. After an analysis of the temporal features present in the layers BiLSTM8 and BiLSTM9, respectively, the output of BiLSTM9 has been sent to an FCL FC2 for further categorization. Finally, the SoftMax layer determines the probability score and predicts the class of the test data based on the trained model. While training the classifier overfitting is the common issue. Thus, its random assignment of hyperparameters may result in overfitting, and the model's performance will decline dramatically. Therefore, in our proposed model, we use the expertise of the Harris Hawk Optimizer technique to finetune parameters in order to help counteract overfitting (30). In order to locate the most relevant target within the extensive search field, this process is implemented. The fundamental purpose of the training is to reduce the process loss function while increasing its accuracy function in diabetic retinopathy prediction.

Experimental setup and results

This section provides a description of the dataset, as well as an overview of the experimental setup and the results that were obtained.

Dataset summary

To evaluate the effectiveness of the proposed approach, we applied it to data from Kaggle's APTOS 2019 Blind Detection Challenge benchmark dataset (31). In Table 2, we can see that various images in the collection have varying degrees of DR.

The effectiveness of a DR categorization task was assessed across all experiments by training and testing with the dataset split 8:2. Additionally, all images have been resized to 256x256 for efficient feature computing.

Performance measures/ evaluation indicators

In order to prove that the proposed model is effective in identifying the DR severity level, this work employs a number of statistical measures, including Sensitivity (SE), Specificity (SP), F-measure, Accuracy, and Kappa.

The following assessment techniques are used to report the findings of the aforementioned diagnostic models: The initial step is to implement comparison and assessment measures such as sensitivity, specificity, accuracy and precision as well as the F1 and Matthew's correlation coefficient (MCC). Finally, the accuracy of the model's classification is shown by computing the area under the receiver operating characteristic curve (AUC) and the ROC curve. These metrics have been explained in detailed below:

Experimental results

In this section experiments are detailed to present the efficiency of proposed model which is the feature extraction of our HHO-CBL model.

Tab. 2. Summary of the Kaggle APTOS 2019 dataset challenge for categorizing DR severity.

Levels based on the degree of intensity of the condition	Samples
Normal (class-0)	1805
Mild (class-1)	370
Moderate (class-2)	999
Severe (class-3)	193
Proliferate (class-4)	295

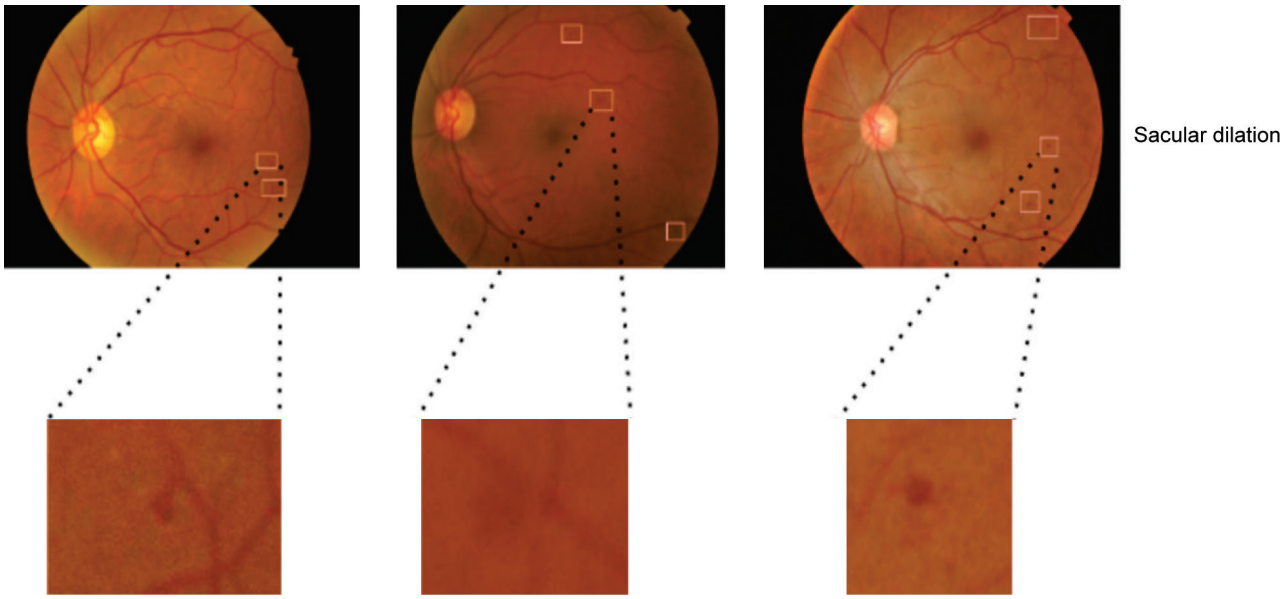

Fig. 2. Reflect features of the splitting of blood vessels as well as a visible capillary network and blood filling the big aneurysm.

In this section experiments are detailed to evaluate the efficiency of Advanced HHO-CBL framework, the various studies have been carried out on the retinography dataset. In the following section, we showcase the objective and quantitative outcomes of many studies including suggested HHO-CBL technique for choosing the most relevant retinal samples, segmenting DR candidate areas or lesions, and classifying DR into five severity levels. The next sections provide an in-depth explanation of the computational methods used to conduct these studies.

Experiment 1: Assessment of the model for the pre-diagnosis of DR

In this experiment, we show an early phase of the development of a microaneurysm that was initially due to a splitting of the capillary basement membrane, saccular dilation, progressive accumulation of a hyaline-like material in the capillary aneurysm wall, and retinal swelling due to kinking of vessels. These circumstances are associated with the earliest stages of MNPDR. Figure 2 demonstrates splitting of blood vessels and visible capillary network and blood fills the large aneurysm. Figure 3 shows

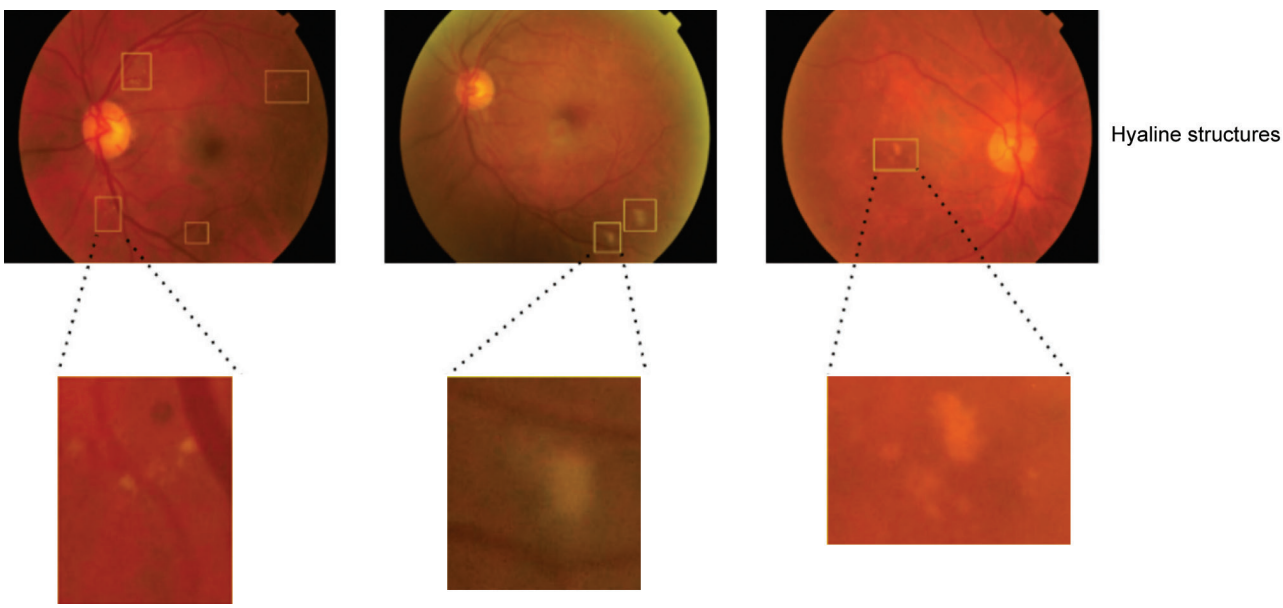

Fig. 3. Illustrate the hyaline structures that are present in the aneurysm.

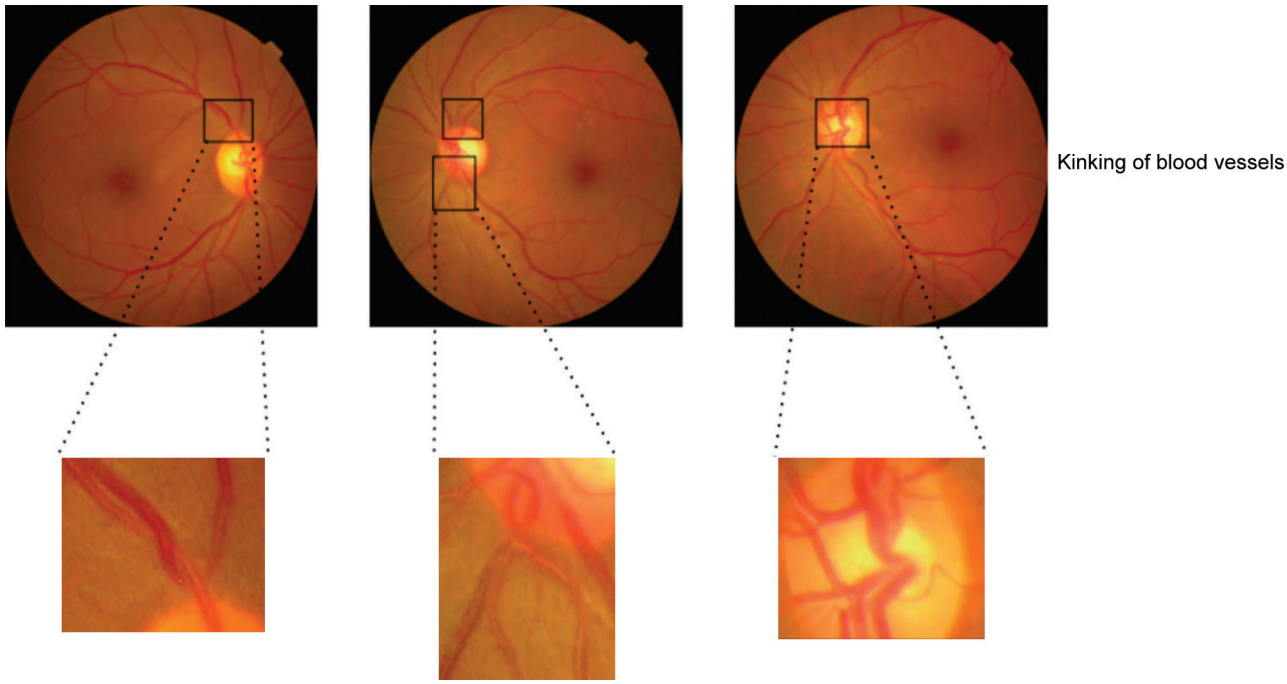

Fig. 4. Exhibit enlargement of the retina as well as kinking of the veins.

Tab. 3. Performance of the Recommended HHO-CBL Model on 3,662 Images Representing Five Dr Severity Levels and Prediagnosis Stage.

Classes	Severity level	SE (%)	SP (%)	F1-score (%)	MCC (%)	Kappa	ACC (%)
0	Normal	95.4	98.4	99.4	95.9	92.0	99
1	MPDR	93.2	96.6	98.0	93.7	90.6	97.0
2	NPDRM	93.9	96.9	98.5	94.4	90.7	97.7
3	SPDR	94.2	97.6	99.0	94.7	91	98.0
4	PDR	95.2	98.5	99.2	95.5	91.8	98.8
5	Pre-Early	92.9	96.1	97.2	93.4	88	96.4

hyaline structures of the aneurysm. However, such abnormal nerve fibers have been seen at early stage within the diabetic aneurysms. The Figure 4 depicts a capillary and a tiny vein in the same diabetic retina that have become interconnected like a bridge. There is swelling and degeneration of neural structures in the retina here.

From Table 3 we can show that in order to evaluate the effectiveness of the HHO-CBL system for the classification of pre-early diagnosis of Mild NPDR, statistical analysis of SE, SP, Precision, F-measure, Matthew's correlation coefficient (MCC), and Accuracy were performed on 3662 photographs. As can be seen in the Figure 5, the pre-Early stage has an impressive 96.6 % accuracy after 50 epochs and produced AUC.

Experiment 2: Model assessment for DR classification

The various levels of DR, as seen in the Figure 6, are evaluated and contrasted in this section. To ascertain the efficacy of the HHO-CBL system in categorizing each NPDR and PDR classes for DR diagnosis, 3,662 specialized digital retinal samples were subjected to statistical analysis based on SE, SP, Precision, F-measure, Matthew's correlation coefficient (MCC) and Accuracy. Table 4 reports a marked improvement of the stated HHO-CBL architecture for normal class (SE: 95.4 %, SP: 98.4 % and F-measure: 99.4 %, and accuracy: 99 %), mild diabetes class (SE: 93.2 %, SP: 96.6 %,

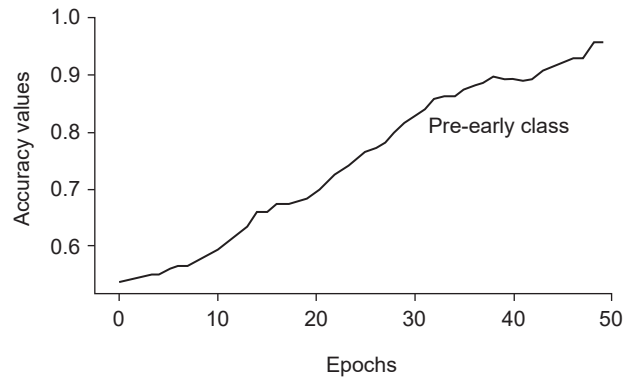

Fig. 5. Epoch-Accuracy for pre-Early diagnosis using HHO-CBL Model.

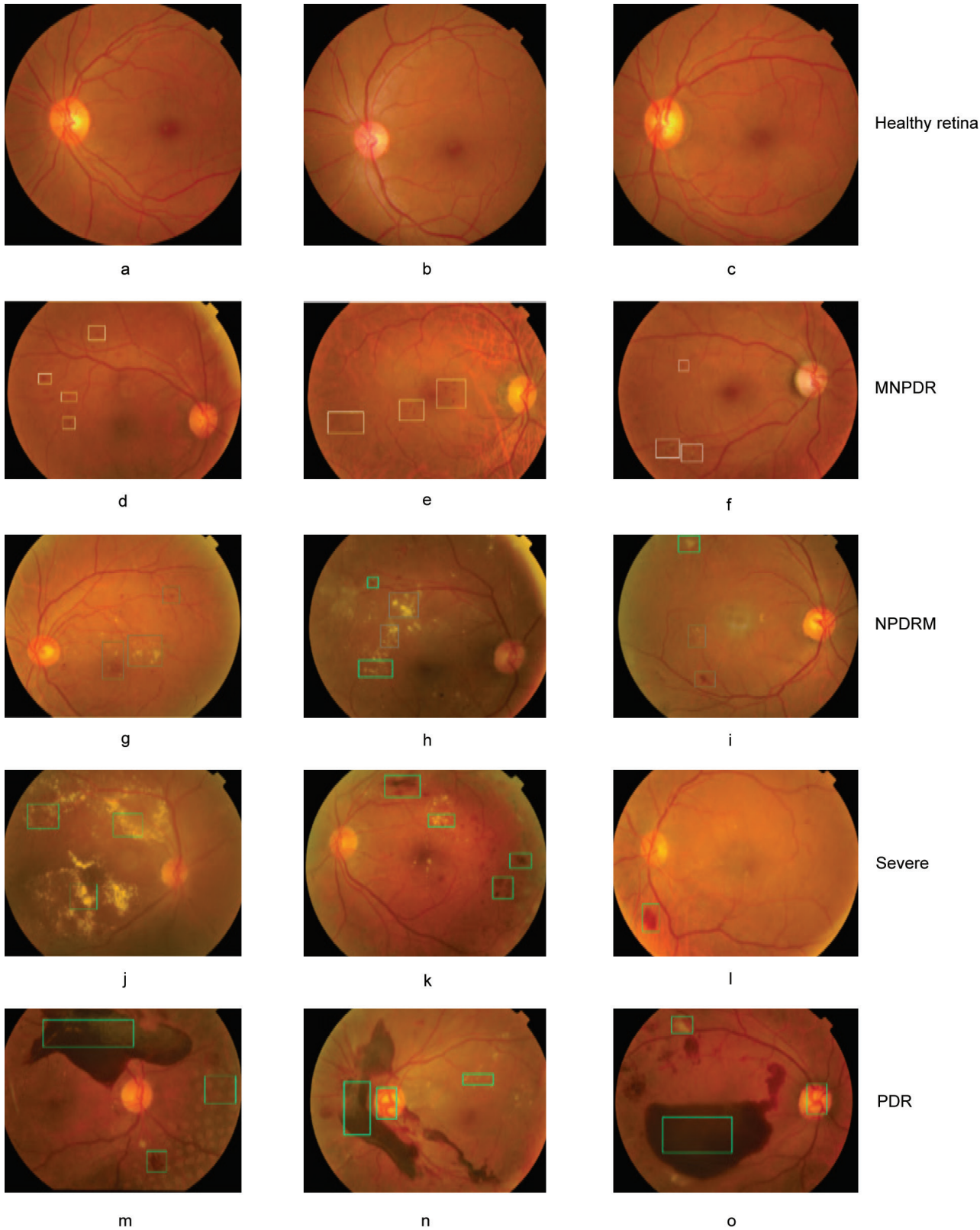

Fig. 6. Classification of Different Levels of DR to Normal to PDR using Proposed Model.

F-measure: 98 %, and Accuracy: 97.0 %) compared to moderate diabetes class (SE: 93.9 %, SP: 96.9 %, F-measure: 98.5 %, and Accuracy: 97.7 %), severe diabetes class (SE: 94.2 %, SP: 97.6 %, F-measure: 99.0 %, and accuracy: 98.0 %) and Proliferative DR (SE: 95.2 %, SP: 98.5 %, F-measure: 99.2 %, and accuracy: 98.8 %). Figure 7 clearly demonstrated the highest accuracy with 50 number of epochs.

Figure 8 depicts the ROC curve that was generated by our HHO-CBL model. The ROC curve and the AUC value both show how close the prediction is to being a perfect classification. This information is displayed in the upper left-hand corner of the ROC coordinate. The area under the ROC curve is represented by the value of the AUC. The performance of the model improves in proportion to the value's proximity to 1. The Figure 9 displays an area under the curve (AUC) value of 0.99 for the No-DR class, 0.96 for the Mild (MNPDR), 0.97 for the Moderate (NPDRM), and 0.97 for the Severe (SNPDR) and Proliferative DR (PDR) classes, respectively. The area under the curve (AUC) is 0.96 for pre-early diagnosis. As a result of the fact that a morphological variation of the fundus pictures for the Pre-Ealy and MNPDRR grades has an effect on the identification of pathological structures, the AUC of the Pre-Ealy and MNPDRR grades DR is lower than that of the others with 96.00 %.

Experiment 3: Performance comparison of the proposed method with state of the art

In this experiment, upon comparing our model with the basic CNN-Bi-LSTM architecture, the results depicted in Figures 8 and 9 reveal significantly superior accuracy achieved by our suggested model, surpassing the outcomes of the comparative architecture as shown in Figures 9 and 10.

In this experiment, we evaluated the model presented with the most advanced DR severity classification and demonstrated the efficacy of our network by classifying 3,662 photos from the Kaggle APTOS dataset. The results of a comparison of the performance of the model developed and the models used in (16–20) are shown in Table 4. It can be shown from the performance assessment carried out in this study that the technique that is being suggested is significantly more effective than the models that are already present in the relevant research. We similarly acquired a average score of 0.97 on the area under the curve (AUC), but our accuracy score were better than the existing work. Overall, we see that the potential of the proposed HHO-CBL system here easily outperforms the approaches.

Tab. 4. Performance Comparisons with State-of-the-Art Five Severity-Level of DR on the Test Set of Kaggle Aptos Benchmark.

Research study	Precision	Accuracy	AUC	F-score
Nahiduzzaman M et al (16)	0.96	0.92	0.98	–
Shaik NS et al (17)	0.85	0.85	0.97	0.85
Canayaz M et al (28)	0.95	0.95	–	0.95
Imran M et al (19)	0.85	0.92	0.95	–
Islam MRet al (20)	0.73	0.84	0.93	0.70
Traditional CNN-BiLSTM	00.72	0.82	0.84	0.83
HHO-CNN-Bi-LSTM	0.96	0.98	0.97	0.99

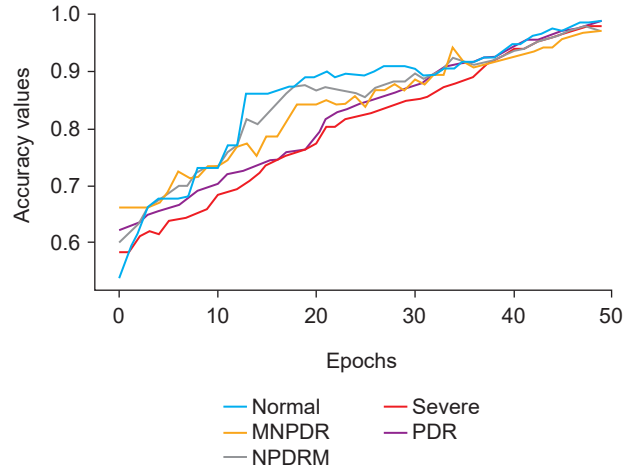

Fig. 7. HHO-CBL Model per epoch accuracy for DR grades.

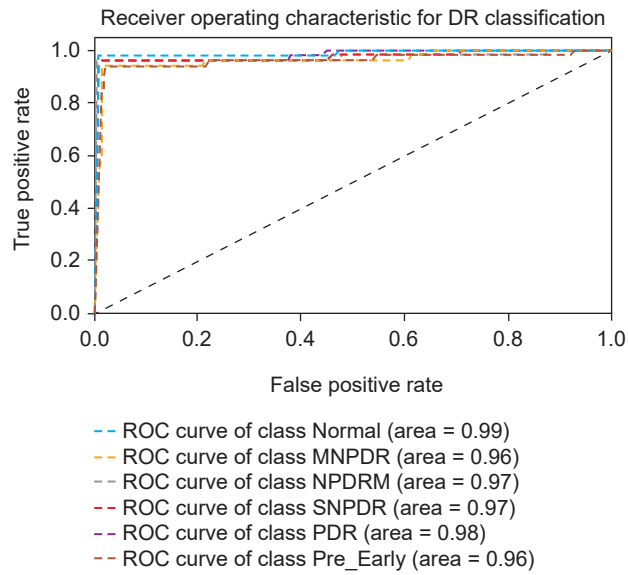

Fig. 8. ROC Curves for the varying degrees of Diabetic Retinopathy severity.

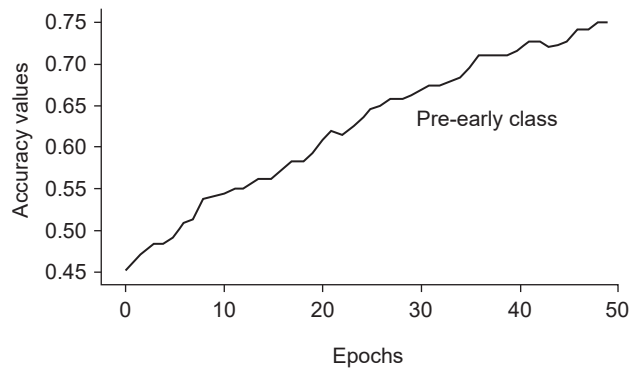

Fig. 9. Accuracy for Pre-Early diagnosis using Original CNN-Bi-LSTM.

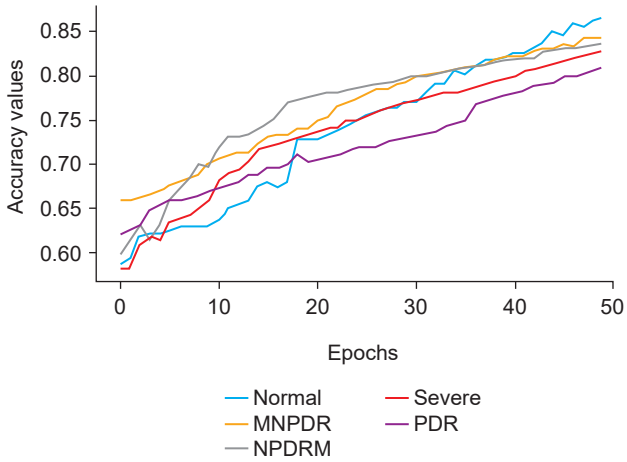

Fig. 10. Accuracy for Grades of DR using Original CNN-Bi-LSTM.

Conclusion

The primary objective of this research is to develop an early effective and reliable classification model for the severity of DR with limited data. In this study, a novel HHO-CBL was designed in order to investigate the major factors that contribute to the development of microaneurysms and to diagnose all five grades of DR. Categorizing the five levels of DR severity through color fundus images is difficult due to the complex structures and appearances of lesions. Existing research primarily focuses on classifying DR from mild to advanced stages, yielding promising results. Prior to inputting the fundus image into the model to learn distinct features, it undergoes resizing, preprocessing, and augmentation. The suggested model employed a Harris Hawk optimization approach for optimal feature selection and hyperparameter finetuning to overcome overfitting and extracted features are classified with an ensemble method of HHO-CBL. The proposed model was trained using 3662 photos from the Kaggle APTOS image benchmark. The training was successful, yielding substantial results in terms of SE, SP, F-measure, precision, MCC, Kappa, AUC and classification accuracy on a test set of 5 images, as appropriately stated in Section 6. Overall, the obtained results presented through the evaluation performance metrics indicates that the pre-early diagnosis and five grade classification using feature embedding technique outperformed the other prevailing approaches.

References

1. **https://www.nei.nih.gov/learn-about-eye-health**/eye-conditions-and-diseases/diabetic-retinopathy#:~:text=Diabetic%20retinopathy%20is%20caused%20by,your%20eye%20(optic%20nerve).

2. **Lin X, Xu Y, Pan X, Xu J, Ding Y, Sun X, Song X, Ren Y, Shan PF.** Global, regional, and national burden and trend of diabetes in 195 countries and territories: an analysis from 1990 to 2025. Sci Reports 2020; 10 (1): 1–11.

3. **Diabetic Retinopathy**: https://www.mayoclinic.org/diseasesconditions/diabeticretinopathy/symptoms-causes/syc-20371611.

4. **Conditions of Diabetic Retinopahthy**: https://manochaeyehospital.com/services/diabetic-retinopathy/.

5. **Diabetic Retiopathy**: https://www.aoa.org/healthy-eyes/eye-and-vision-conditions/diabetic-retinopathy?sso=y.

6. **Guide for DR**: https://www.dishaeye.org/blog/diabetic-retinopathy-guide/.

7. **Grzybowski A, Brona P, Lim G, Ruamviboonsuk P, Tan GS, Abramoff M, Ting DS.** Artificial intelligence for diabetic retinopathy screening: a review. Eye 2020; 34 (3): 451–460.

8. **Huang S, Li J, Xiao Y, Shen N, Xu,T.** RTNet: Relation transformer network for diabetic retinopathy multi-lesion segmentation. IEEE Transactions on Medical Imaging. 2022.

9. **Manan MA, Khan TM, Saadat A, Arsalan M, Naqvi SS.** A Residual Encoder-Decoder Network for Segmentation of Retinal Image-Based Exudates in Diabetic Retinopathy Screening. arXiv preprint arXiv:2201.05963, 2022.

10. **Abdel Maksoud E, Barakat S, Elmogy M.** Diabetic retinopathy grading system based on transfer learning. arXiv preprint arXiv 2012.12515.

11. **Pao SI, Lin HZ, Chien KH, Tai MC, Chen JT, Lin GM.** Detection of diabetic retinopathy using bichannel convolutional neural network. J Ophthalmol 2020.

12. **Yang Yehui, Tao Li, Wensi Li, Haishan Wu, Wei Fan, Wensheng Zhang**. Lesion detection and grading of diabetic retinopathy via two-stages deep convolutional neural networks. In International conference on medical image computing and computer-assisted intervention, pp. 533–540. Springer, Cham, 2017.

13. **Tang MCS, Teoh SS.** November. Blood vessel segmentation in fundus images using Hessian matrix for diabetic retinopathy detection. In 2020 11th IEEE Annual Information Technology, Electronics and Mobile Communication Conference (IEMCON) 2020; 0728–0733).

14. **Ai Z, Huang X, Fan Y, Feng J, Zeng F, Lu Y.** DR-IIXRN: detection algorithm of diabetic retinopathy based on deep ensemble learning and attention mechanism. Front Neuroinformat 2021; 15.

15. **Xu L, Wang L, Cheng S, Li Y.** MHANet: A hybrid attention mechanism for retinal diseases classification. Plos One 2021; 16 (12): e0261285.

16. **Nahiduzzaman M, Islam MR, Goni MOF, Anower MS, Ahsan M, Haider J, Kowalski M.** Diabetic Retinopathy Identification Using Parallel Convolutional Neural Network Based Feature Extractor and ELM Classifier. Exp Systems Appl 2023; 119557.

17. **Shaik NS, Cherukuri TK.** Hinge attention network: A joint model for diabetic retinopathy severity grading. Applied Intelligence 2022; 52 (13): 15105–15121.

18. **Canayaz M.** Classification of diabetic retinopathy with feature selection over deep features using nature-inspired wrapper methods. Appl Soft Computing 2022; 128: 109462.

19. **Imran M, Ullah A, Arif M, Noor R.** A unified technique for entropy enhancement based diabetic retinopathy detection using hybrid neural network. Computers Biol Med 2023; 145: 105424.

20. **Islam MR, Abdulrazak LF, Nahiduzzaman M, Goni MOF, Anower MS, Ahsan M, Haider J, Kowalski M.** Applying supervised contrastive learning for the detection of diabetic retinopathy and its severity levels from fundus images. Computers Biol Med 2023; 146: 105602.

21. **Miroaneurysms in Diabetic Retinopathy**: https://www.medicalnewstoday.com/articles/microaneurysms-diabetic-retinopathy#summary.

22. **Wolter JR.**. Diabetic capillary microaneurysms of the retina. Arch Ophthalmol 1961; 65 (6): 847–854.

23. **Hessian Matrix**: https://machinelearningmastery.com/a-gentle-introduction-to-hessian-matrices/.

24. **Alabool HM, Alarabiat D, Abualigah L, Heidari AA.** Harris hawks optimization: a comprehensive review of recent variants and applications. Neural Computing Applications 2021; 33: 8939–8980.

25. **Heidari AA, Mirjalili S, Faris H, Aljarah I, Mafarja M, Chen H.** Harris hawks optimization: Algorithm and applications. Future Generation Computer Systems 2019; 97: 849–872.

26. **El-Hag NA, Sedik A, El-Shafai W, El-Hoseny HM, Khalaf AA, El-Fishawy AS, Al-Nuaimy W, Abd El-Samie FE, El-Banby GM.** Classification of retinal images based on convolutional neural network. Microscopy Res Techniq 2021; 84 (3): 394–414.

27. **Too J, Liang G, Chen H.** Memory-based Harris hawk optimization with learning agents: a feature selection approach. Engineering Computers 2022; 38 (Suppl 5): 4457–4478.

28. **Wahid MF, Hossain AA.** July. Classification of Diabetic Retinopathy from OCT Images using Deep Convolutional Neural Network with BiLSTM and SVM. In: 2021 12th International Conference on Computing Communication and Networking Technologies (ICCCNT) (pp. 1–5).

29. **Dureja A, Pahwa P.** Analysis of non-linear activation functions for classification tasks using convolutional neural networks. Recent Patents on Computer Sci 2019; 12 (3): 156–161.

30. **Rajendran S, Khalaf OI, Alotaibi Y, Alghamdi S.** MapReduce-based big data classification model using feature subset selection and hyperparameter tuned deep belief network. Scie Reports 2021; 11 (1): 24138.

31. **https://www.kaggle.com/datasets/mariaherrerot**/aptos2019?select=train_images.

Received June 8, 2023.
Accepted August 18, 2023.